Journal of Hydrology 663 (2025) 134294

Contents lists available at ScienceDirect

Journal of Hydrology

journal homepage: www.elsevier.com/locate/jhydrol

Research papers

The impact of declining rainfall and ocean forcing on morphology and dynamics of an island fresh groundwater lens, South-West Western Australia

S. Sharifazari [a,b,*], J. McCallum [c], K. Meredith [d], F. Johnson [b,e], J.G. Palmer [f], C.S.M. Turney [g], M.S. Andersen [a]

[a] Water Research Laboratory, School of Civil and Environmental Engineering, University of New South Wales, Australia
[b] Water Research Centre, School of Civil and Environmental Engineering, University of New South Wales, Australia
[c] College of Science and Engineering, Flinders University, Adelaide, South Australia 5042, Australia
[d] Australian Nuclear Science and Technology Organisation (ANSTO), New Illawarra Rd, Lucas Heights, NSW 2234, Australia
[e] ARC Training Centre in Data Analytics for Resources and Environments (DARE), Australia
[f] School of Environmental and Life Sciences, College of Engineering, Science and Environment, University of Newcastle, Australia
[g] Division of the Deputy Principal Research and Impact, Heriot-Watt University, Edinburgh, Scotland, UK

ARTICLE INFO

This manuscript was handled by Renato Morbidelli, Editor-in-Chief

Keywords:
3D density-dependent groundwater model
Rainfall recharge
Rottnest Island
Water resource management

ABSTRACT

Fresh groundwater lenses are an important natural source of potable water for communities on small oceanic islands but are highly vulnerable to climate variability and long-term trends such as prolonged decadal rainfall decline. This is particularly true of the islands along the coast of Southwest-Western Australia located in the Indian Ocean where substantial rainfall declines are the primary driver of a reduction in the volume of groundwater recharge. On these islands, the impact of these changes is further complicated by seawater mixing associated with sea level fluctuations operating on time scales ranging from hourly to seasonal, interannual, and decadal. The complex interaction between climatic and sea level variability highlights the need for well-constrained density-dependent groundwater models to understand changes to recharge on various timescales to manage groundwater resources. This study focused on Rottnest Island where groundwater age data was combined with water level and salinity measurements to develop a 3D density-dependent groundwater model. The steady state modelling of the fresh groundwater lens suggests a recharge rate of −41 % of the long-term historic annual rainfall, with the winter rainfall important for lens recharge, suppressing the upward movement of the saline transition zone groundwater associated with seasonal sea level fluctuations. A transient simulation reveals a substantial reduction of up to 50 % in the volume of potable groundwater (i.e. in the freshwater lens) in response to the prolonged rainfall decline that started in the late 1960s combined with groundwater abstraction. The sustained regional winter rainfall decline experienced in the Southwest Australia region accounts for most of this reduction when considering transient sea level boundary conditions. The modelling approach used in this study for Rottnest Island offers insights that can be applied to other oceanic islands experiencing changing climatic forcings, particularly in regions where sea level variability plays a significant role.

1. Introduction

In coastal zones, fresh aquifers are the primary source of potable water to more than one billion people (Siegel, 2020; Small and Nicholls, 2003). Due to their proximity to oceans, the freshwater contained in these aquifers are vulnerable to seawater intrusion exacerbated by sea level rise and reduced rainfall recharge as consequences of global climate change. This is especially true for small oceanic islands with limited surface water catchment areas and aquifer storage (Jiao and Post, 2019; Werner et al., 2017; White and Falkland, 2010).

Most small oceanic island communities rely on limited freshwater sources stored within a thin groundwater lens situated on top of denser

* Corresponding author at: Water Research Laboratory, School of Civil and Environmental Engineering, University of New South Wales, Australia.
E-mail address: s.sharifazari@unsw.edu.au (S. Sharifazari).

https://doi.org/10.1016/j.jhydrol.2025.134294
Received 14 May 2025; Received in revised form 16 September 2025; Accepted 17 September 2025
Available online 20 September 2025

saline water. The size of the fresh groundwater lens is affected by rainfall recharge, which is often the sole source of fresh water to replenish the lens (White and Falkland, 2010). Reduced rainfall recharge results in a decreased volume of freshwater. This is because a reduction in fresh recharge water decreases the thickness of the freshwater lens and lowers the hydraulic gradient, resulting in increased seawater intrusion (Holding and Allen, 2015). Thus, understanding lens response to changes in recharge and its variability is essential to manage and protect freshwater on oceanic islands.

In addition to rainfall, other dynamic forces, such as sea level fluctuations, significantly impact the volume of freshwater in the groundwater lens and thereby obscure its response to recharge variability. Tidal fluctuations have been suggested to amplify seawater intrusion and create a thicker transition zone with a greater impact on the regions near the shore (Ataie-Ashtiani et al., 1999; Holt et al., 2019; Pool et al., 2014; Sheng et al., 2020). Unlike tides, for which their influences diminish with distance rapidly, seasonal and interannual sea level fluctuations attenuate slowly (Cantelon et al., 2023; Haehnel et al., 2024; Heiss and Michael, 2014; Michael et al., 2005; Wood and Harrington, 2015), penetrating further into the aquifer and exerting considerable impacts on inland salt distribution. Such low-frequency sea level fluctuations are prominent in areas such as the Indian Ocean, i.e., off India and along the coast of Western Australia, and South China Sea (Lowe et al., 2021).

In the Indian Ocean, climate induced recharge reduction is the primary driver for freshwater lens depletion as demonstrated by hydrochemical evidence from both low-lying coral (Chattopadhyay and Singh, 2013) and elevated carbonate (Bryan et al., 2016) islands. For example, Bryan et al. (2016) used water isotope tracers to infer groundwater responses and reported that a −20 % rainfall reduction since 1977 has led to freshwater lens shrinkage by 30 % on Rottnest Island due to enhanced seawater intrusion. If high-frequency groundwater level data is available, the forces affecting the freshwater lens, including recharge, can be disentangled (Haehnel et al., 2024). However, the corrected water level measurements can only reveal the immediate groundwater level response, and without accounting for flow and salt transport, they are insufficient to resolve the 3D freshwater distribution and the dynamic evolution of the freshwater lens. In this context, geophysical surveys are a valuable tool for spatial mapping of the subsurface water salinity distribution across islands or coastal areas and complementing water level and chemistry data obtained from monitoring wells (Banks et al., 2024). Such techniques may further support the calibration of groundwater models by characterizing the freshwater lens geometry beyond the limited spatial information from boreholes (Briggs et al., 2021; Pavlovskii et al., 2022). Numerical coupled subsurface flow and mass transport modelling techniques have proven to be effective tools in providing a reliable estimation of these responses (Bear, 2004; Sulzbacher et al., 2012).

The reliability of numerical models, however, depends heavily on the available data and the model calibration. Despite advancements in groundwater measurements, the use of measured hydraulic heads still remains the most common approach to calibrating numerical models (Dibaj et al., 2020). Importantly, including one or more additional types of groundwater observation, such as groundwater age, mass and water fluxes, temperature, or tracer concentration, in the calibration stage has been found to significantly reduce the uncertainty of predictions made by the groundwater models (Delsman et al., 2016; Schilling et al., 2019). Groundwater age, in particular, has proven to be an effective calibration tool in numerical groundwater modelling (Sanford, 2011), and its application in calibrating density-dependent numerical models for coastal aquifers has been demonstrated in recent studies (Holt et al., 2021; Reznik et al., 2021).

The early application of numerical models in island settings primarily focussed on estimating sustainable yields from the freshwater lens (Ghassemi et al., 1998) but more recently have been applied to address the impacts of climate change, including sea level rise (Alsumaiei and Bailey, 2018; Chui and Terry, 2013), flooding impact (Frederiks et al., 2024; Liu and Tokunaga, 2020), and recharge changes (Holding and Allen, 2015; Puigserver et al., 2024; Sulzbacher et al., 2012; Werner et al., 2017). Among climate change impacts, groundwater recharge reduction is of great concern for accelerating seawater intrusion and freshwater lens reduction in small islands worldwide (Holding et al., 2016; Puigserver et al., 2024). While most modelling studies have investigated the individual effects of recharge and sea level changes (Banks et al., 2024; Chui and Terry, 2013; Liu and Tokunaga, 2020; Pool et al., 2014; Tang et al., 2020), few studies have explicitly addressed the combined effects of these forces on freshwater lens dynamics (Frederiks et al., 2024; Heiss and Michael, 2014; Sheng et al., 2020; Wood and Harrington, 2015). Although these studies documented the importance of seasonal sea-level fluctuations for coastal-aquifer behavior, they generally used two-dimensional models and did not quantify—nor disentangle—the relative contributions of seasonal sea-level variability vs recharge to island-scale lens thickness and transition-zone dynamics. Two-dimensional models can suffice when a representative cross-section captures the main dynamics, but on islands with curved shorelines, internal lakes, and distributed pumping a 3-D model is required to resolve lens thickness and mixing. Simulating the interaction between declining recharge and sea level fluctuations to resolve 3D freshwater distribution requires computationally extensive transient simulation of a fully resolved sea level signal acting on a coastal boundary (Haehnel et al., 2023).

To better understand the relative influences of tidal and seasonal sea level fluctuations and recharge changes on freshwater lenses, regression deconvolution and 3D density-dependent groundwater modelling techniques are used in this study. Groundwater level measurements are used to understand the role of oceanic, climatic, and anthropogenic forces on freshwater lens variability on Rottnest Island. TDS measurements and environmental isotopic tracers in groundwater are used to develop a 3D density-dependent groundwater model. The issue of computational tractability of the model is addressed by creating a smaller truncated modelling domain to permit transient simulations. Finally, the model is used to interpret the effects of rainfall recharge variability on the fresh groundwater source, information that can be used to manage freshwater resources for the region.

2. Methods

2.1. Hydrological and geological setting

Rottnest Island is a small carbonate island located off the coast of southwest Australia, about 18 km west of the city of Perth. Around 500,000 tourists visit Rottnest each year, which substantially raises the need for fresh water on the Island (Bryan et al., 2016). Rottnest Island has a Mediterranean-like climate, characterized by mild, wet winters and warm to hot, dry summers (Seager et al., 2019; Urdiales-Flores et al., 2023). It receives a mean annual rainfall of 680 mm (1880–2023), of which 80 % falls in winter between May and September. The yearly potential evapotranspiration for the island is estimated to be about 1694 mm (Bryan et al., 2017). To maximize groundwater recharge, a revegetation program was implemented in the central part of the island by removing weeds and replanting with native vegetation (Bryan et al., 2016).

Fig. 1 shows the topography of the island and its surficial geology overlain by the estimated freshwater lens areas (Playford, 1976). The island has an area of about 19 km^2, with salt lakes covering 10 % of the island (Fig. 1b). Rottnest has similar geology to other carbonate aeolianite islands such as Bermuda and the Bahamas, characterized by dune-shaped topography and distinct geological features, such as elevated ridges and layers containing marine fossils. Rottnest Island has a maximum elevation of 46 m and is about 4.5 km wide (Fig. 1a). Pleistocene to mid-Holocene carbonate aeolianite (Tamala limestone) forms the underlying composition of the island (Playford, 1976). The geology of the island is dominated by the Tamala limestone with a thin

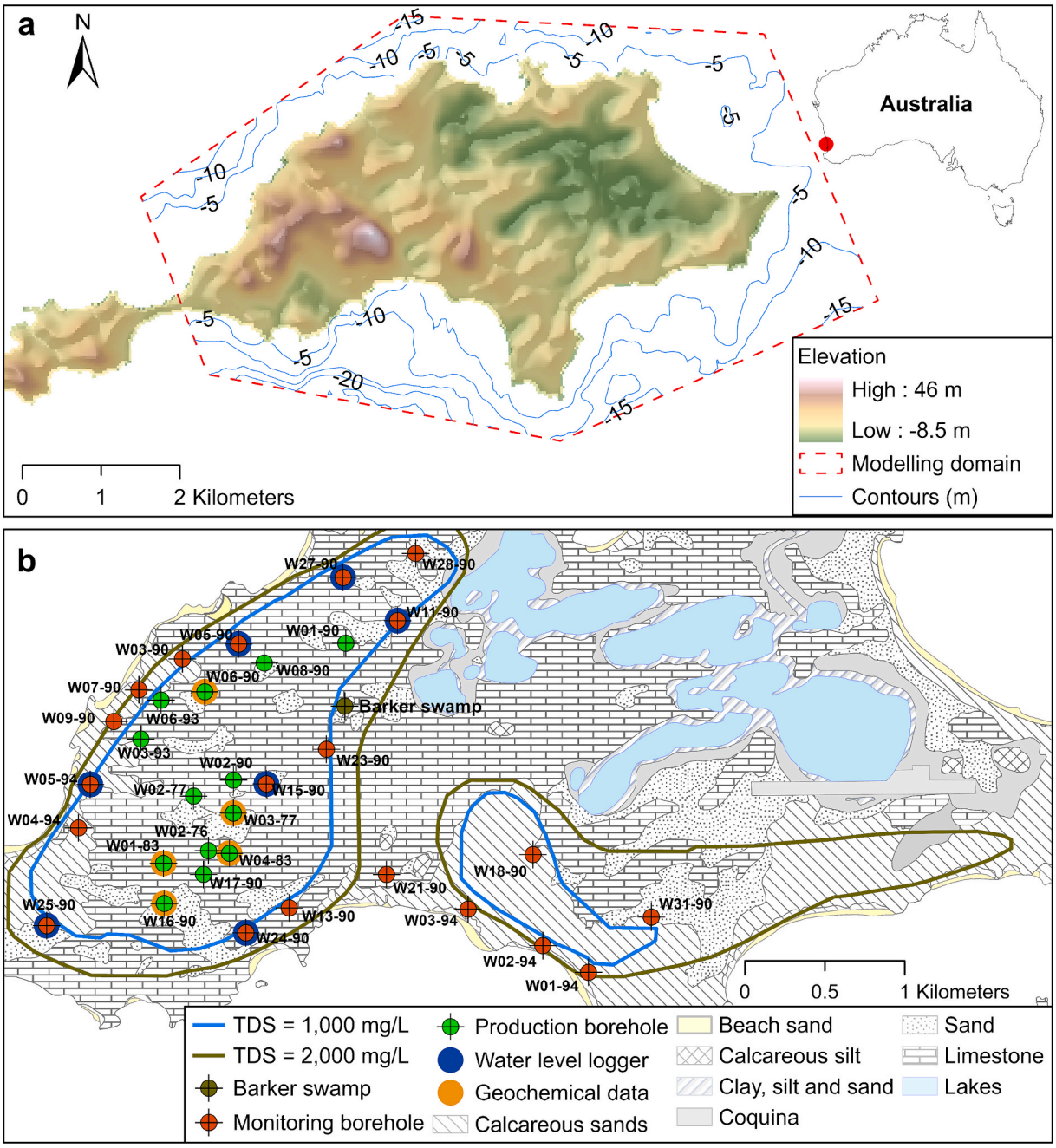

Fig. 1. (a) Rottnest Island's location (red point on inset), its surface topography with nearshore bathymetric contours (−5, −10, −15 m AHD), and the groundwater modelling domain in this study. (b) The surficial geology of Rottnest Island overlain by the initial freshwater lens areas detected in 1976 (Playford, 1976). The red and green circles represent the location of monitoring and production wells. (For interpretation of the references to colour in this figure legend, the reader is referred to the web version of this article.)

intercalated layer of Last Interglacial coral reef (Rottnest Island limestone) and overlying Holocene Herschell Limestone around margins of the salt lakes, indicating a relative higher sea level in the past (Playford, 1976). Two groundwater lenses were identified by Playford (1976), with the larger one located in the west of the island (Fig. 1b), which has been used as the source of potable water since 1977.

The approximately 115 m thick Tamala limestone layer is highly permeable with a matrix porosity of 0.3–0.5, and a hydraulic conductivity ranging from 100 to 2000 m/day. The system is weakly cemented and characterized by dual porosity in which numerous connected channels are presented within a matrix of interparticle porosity (Smith et al., 2012). However, the extensive dissolution of aeolianites with high initial porosity suggests a matrix flow dominated groundwater system (Bryan et al., 2020), justifying modelling groundwater flow and transport as a porous media on Rottnest Island. As the detailed stratigraphic information and borehole lithologic logs were not available and the Tamala limestone is by far the dominating formation, the geological model of the island was simplified to a homogeneous one-layer aquifer similar to the model developed for Quinns Rocks, 35 km north of Perth (Costall et al., 2020).

2.2. Groundwater data

More than 30 monitoring and production boreholes have been used to monitor and abstract groundwater from the freshwater lens on Rottnest Island. While the production boreholes are concentrated in the

lens area, several monitoring boreholes have been constructed both within and around the lens area since 1990. Table S1 summarizes bore metadata. Groundwater levels and TDS were measured at irregular intervals from 1976 to 1995 for some of these boreholes. Continuous groundwater levels (half hourly intervals) were measured using Solinst Gold Loggers in seven monitoring bores from September 2014 to February 2017. All groundwater level measurements were referenced to the Australian Height Datum (AHD) and corrected for barometric pressure (Bryan, 2017). Comprehensive water chemistry and isotopic samples were also obtained from field campaigns conducted in September 2014, March 2015, September 2015, and March 2016 (Bryan et al., 2020).

2.3. Dynamic forces influencing the freshwater lens

A range of natural and anthropogenic drivers influence the freshwater lens on small oceanic islands, with recharge, sea level fluctuation, and groundwater abstraction being among the most important factors.

Rainfall recharge has been identified as the only freshwater source entering the groundwater system on Rottnest Island (Bryan et al., 2016). Methods such as chloride mass balance, renewal rate, and water mass balance have been used to estimate groundwater recharge on Rottnest Island, with the chloride mass balance method found to underestimate rainfall recharge on Rottnest (Bryan et al., 2016; Leech, 1977). Water isotope tracers, tritium (^{3}H), deuterium ($\delta^{2}H$), and oxygen-18 ($\delta^{18}O$) have also been used to estimate the groundwater residence time and thereby understand groundwater response to changes in rainfall recharge (Bryan et al., 2020). To provide initial daily recharge input to the groundwater model in this study, the water balance model developed by Bryan et al. (2016) was modified to include the soil water storage as detailed in the supplementary text S3.

Groundwater abstraction during the peak season for water demand in austral summer (December and January), decreases the water levels, particularly near the production boreholes. The first production borehole was constructed in 1976, and groundwater abstraction ceased in 2017. During this period the production boreholes supplied around 25 % – 65 % of Rottnest's potable water, with a maximum constant rate of 17 m^3/day per borehole during summer months (Department of Water, 2014; Playford, 2004). Table S1 summarizes the average amount of water supplied to Rottnest Island during 1977–2017.

Groundwater level measurements from the monitoring boreholes are highly responsive to sea level fluctuations (Bryan et al., 2016). This makes it difficult to understand and quantify the influence of climate variability on recharge and the lens response. Spectral analyses of groundwater level data reveal variabilities within semi-diurnal and diurnal tidal frequencies (Fig. 2). Regional nontidal seasonal and interannual sea level variability driven by climatic and oceanic forces (Lowe et al., 2021) are also reflected in the groundwater level data.

To understand the impact of rainfall recharge, we followed the method set out in Haehnel et al. (2024) using regression deconvolution to disentangle the sea level influence on observed groundwater level data. This analysis is detailed in Supplementary text S1. The resulting disentangled sea-level series were used in a set of model simulations designed to evaluate the relative roles of recharge and sea-level variability on lens thickness and transition-zone dynamics. The model simulations employed different combinations of forcings, including zero recharge, water-balance-derived recharge, constant sea level, variable sea level, and variable sea level without its seasonal component.

2.4. Numerical 3D groundwater flow and transport model

The finite element subsurface FLOW system (FEFLOW 8.0) code was used to solve the coupled density-dependent flow and solute transport equations for Rottnest Island. The governing equations of the system are described in detail in Diersch (2013). FEFLOW has previously been used to model subsurface systems and seawater intrusion in many island settings (Costall et al., 2020; Liu and Tokunaga, 2020; Pavlovskii et al., 2022; Sulzbacher et al., 2012). FEFLOW provides the capabilities to calculate groundwater age and allows for flexible mesh structures which are required for complex boundaries such as lake boundaries in the study area.

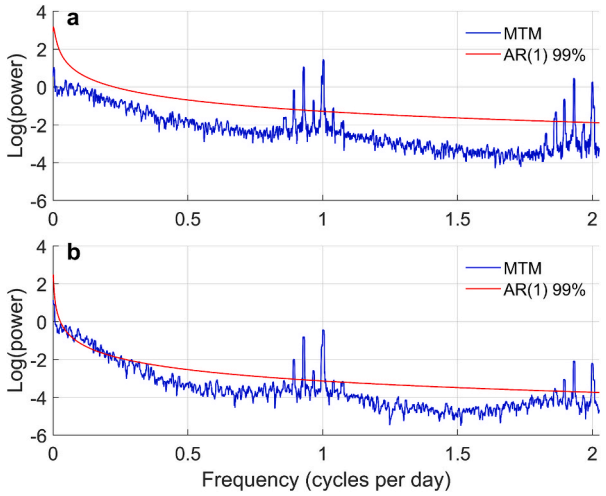

Fig. 2. Multitaper spectral analysis of (a) sea (Hillarys, 25 km east of Rottnest) and (b) groundwater level measurements in borehole W05-94 on Rottnest Island. The red line indicates the 99 % confidence when using an AR(1) red noise model. The results for other boreholes are similar to that of borehole W05-94. (For interpretation of the references to colour in this figure legend, the reader is referred to the web version of this article.)

2.4.1. Modelling domain and boundary conditions

The modelling domain covered the lens extent identified by Playford (1976) and extended further into the Indian Ocean (Fig. 1a). The inclusion of a buffer zone into the ocean allowed the model to capture all the important seawater-freshwater interactions (Sulzbacher et al., 2012) and allowed for a sub-sea zone of groundwater discharge and seawater intrusion below. The western tip of the island, where there is no monitoring data, was excluded from the model and the domain was truncated at the narrowest part of the island. To set up the three-dimensional numerical groundwater model, the domain was vertically extended from the land surface (up to 45 m above sea-level) to 70 m below sea level, covering the portion of the −115 m thick Tamala Limestone located below sea-level. Topographic and bathymetric maps from Geoscience Australia were used for the top surface (slice) of the model, including the island's surface, and ocean bathymetry and lakes floors. The model domain was discretized using triangular prism elements (ranging from 25-170 m width) for the horizontal discretization and 32 vertical layers (ranging from 0.5-5 m thick). A detailed description of the discretization is described in the supplementary text S2.

The model's boundary conditions were selected to reflect the hydrogeologic setting of the island. Since the island's mostly steep coastline limits extensive inundation, constant mass and head boundary conditions were applied to all offshore edges and submerged areas of the domain. For the smaller, truncated version of the model, the offshore boundary was replaced with a temporally variable boundary. Seepage faces were added along lake margins, Barker Swamp, and shallow nearshore areas to allow groundwater to naturally discharge. Daily rainfall recharge derived from a water balance model was applied to the land surface, i.e., the top layer of the model, and a no-flow/no-mass-flux boundary was applied to the bottom of the model. Full details, data sources, and justification for this setup are provided in the supplementary text S3, with Fig. S2 showing the applied boundary conditions used.

2.4.2. Initial conditions and model calibration

As there is no information available for Rottnest Island prior to 1976, the freshwater lens was considered to be in a steady state and represented by the lens area first described in 1976 by Playford (1976). The initial model conditions to obtain this quasi-steady state were set to reflect a hypothetical state without a freshwater lens on Rottnest. Thus, 0 mg/L TDS was considered for all saturated media above sea level, and the saturated media below sea level was set to be saturated with seawater with a salinity of 35,000 mg/L. The average recharge rate of 300 mm/year, obtained from trial-and-error within the reported range for annual recharge on Rottnest, was applied to the top slice of the Island domain. The recharge value is close to that obtained from the water balance model and matches the rate of 45 % of long-term annual rainfall determined by Bryan et al. (2016) for the annual effective recharge when considering the median estimation of all used methods. A transient model utilising constant forcings was run to develop an initial condition, determined when changes in mass and head were negligible, i.e., less than 5 % (Banks et al., 2024), between time steps in both flow (hydraulic head) and transport (mass and age) components, representing the extent of the lens in 1976. The result of this simulation was then used as initial condition for the transient calibration. To evaluate the groundwater lens response time after model calibration, an additional steady-state scenario was examined using 50 % of the calibrated recharge rate (i.e., 150 mm/year).

We adopted a staged model calibration consistent with previous modelling studies for island settings (Banks et al., 2024; Frederiks et al., 2024; Sulzbacher et al., 2012), with model calibration undertaken manually in three phases. First, the transient hydraulic model considering abstraction and historical recharge was calibrated against water table data collected in March 2016 as the reference point. In this phase, horizontal hydraulic conductivity and anisotropy ratio were adjusted within the bounds recommended for Tamal limestone in the region (Costall et al., 2020; Smith et al., 2012). The calibrated hydraulic parameters were then used in the calibration of the mass transport model. The transport model was calibrated in steady state against the detected lens extent for the year 1976 and the measured salinity profile for borehole W02-76 in the same year. We adjusted transport parameters, i.e., longitudinal and transvers dispersivity coefficients, within the ranges recommended in previous studies (Anwar and Wawn, 2013; Costall et al., 2020). The third calibration phase was a transient historical matching, where the point-time observations of the state variables were used within the period of 1976 to 2016 to refine the calibrated anisotropy ratio. Pumping rates for this period were set at a maximum rate of 17 m3/day/bore until 1990 (Playford, 2004), and from then, the pumping rate was set to the average rate based on the annual groundwater supply to the Island described in Table S2. This annual groundwater supply was distributed equally between the production boreholes (Fig. 1b), for the annual abstraction period of August to April of the following year (Department of Water, 2014). Tables S2–S4 summarize groundwater abstraction rates, model parameters, and the model set-up for each phase.

2.4.3. Groundwater age simulation

In addition to water level and salinity (TDS), groundwater age data were also used to constrain the calibration. FEFLOW calculates the elapsed time since a parcel of water entered the modelling domain using Goode's method (Diersch, 2013). The method allows a direct simulation of mean groundwater age providing information on travel time and mixing processes using an advection–dispersion transport equation (Goode, 1996). The groundwater residence time was estimated in five boreholes from ^{3}H and $\delta^{18}O$ environmental tracers by Bryan et al. (2020) using a single Lumped Parameter Model (LPM) dispersion model which produced the lowest error among all other available LPMs evaluated in TracerLPM modelling package (Jurgens et al., 2012). These estimates, ranging from a minimum mean age of 11.5 years to a maximum 64.9 years, were used for age calibration in the model here. The maximum age of 64.9 years is an outlier and represents mixed brackish water from the transition zone, which contain older saline water. Residence time increases from the centre toward the margins in the northwestern part of the lens.

3. Results

3.1. Calibration and validation results

Calibration and validation results for the hydraulic and transport models at each phase are detailed in the following sections.

3.1.1. Phase 1: hydraulic calibration

For hydraulic calibration, the measured groundwater level data in March 2016 was converted to the equivalent freshwater hydraulic head using Equation S1, which accounts for density differences. We considered March 2016 as the reference point for our calibration, as more comprehensive data is available for this period. The variability of equivalent freshwater heads is relatively narrow and ranges from −0.02 to 0.57 m, making the calibration challenging given the level of model discretization. Tidal variations also add to this difficulty because water levels fluctuate by 0.06 m in boreholes close to the coast and up to 0.02 m in other boreholes. Using a trial-and-error calibration, the best results were obtained for horizontal and vertical hydraulic conductivities of 125 and 0.5 m/day (Table S3), which is comparable with values from the Tamala Limestone elsewhere (Costall et al., 2020). Fig. 3 compares the modelled hydraulic heads against the measured values accompanied by the colormap representing the equivalent freshwater hydraulic head distribution for the whole modelling domain in March 2016.

The scatter plot shows a reasonable match between measured and modelled values, with a weak but significant correlation (Pearson correlation coefficient (r) = 0.40, p-value = 0.03; r = 0.75 for monitoring boreholes). With the inclusion of production boreholes, the average deviation from measured values, i.e., Mean Absolute Error (MAE), is about 6.5 cm and the Root Mean Square Error (RMSE) is smaller than 10 cm. Although the hydraulic head calibration provides some information about hydraulic properties of the aquifer, calibrating a density-dependent groundwater model separately from mass transport calibration should not be done (Sulzbacher et al., 2012). Thus, the obtained values for hydraulic parameters in this phase may need to be adjusted when calibrating the coupled flow and transport model.

3.1.2. Phase 2: mass concentration calibration

The coupled flow and mass transport model was built based on the hydraulic properties obtained in the previous stage. The model was run in transient mode using the initial and boundary conditions explained in the previous section to reach the steady state representing the mass and hydraulic head distribution in 1976. The model reached steady state condition for the salt mass after 200 years. With hydraulic parameters fixed, we adjusted the transport parameters longitudinal dispersivity (α_L) and its ratio to transverse dispersivity ($\alpha_L : \alpha_T$) from initial ranges of 2–10 m and 10–1,000 (Anwar and Wawn, 2013; Costall et al., 2020) to the calibrated values of 10 m and 400. These changes reduced the W02-76 vertical TDS profile RMS from 9,260 mg/L to 2,715 mg/L and increased the Intersection-over-Union i.e., a metric to calculate the area of overlap (Teixeira et al., 2024), between simulated 1976 lens and Playford (1976) mapped extent from 16 % to 50 %. Fig. 4(a) compares the horizontal TDS distribution obtained from the model for the upper 5 m of groundwater with the 1000 and 2000 mg/L salinity isohalines of the same depth (shown in labelled thick dark green lines) estimated by Playford (1976) (see Figs. 27–18 in Playford (2004)).

The measured TDS gradient for borehole W02-76 in September 1976 is the only groundwater salinity profile available for Rottnest for that year. The vertical profiles of modelled TDS values for different depths were consistent with measured values in borehole W02-76 (Fig. 4(b)).

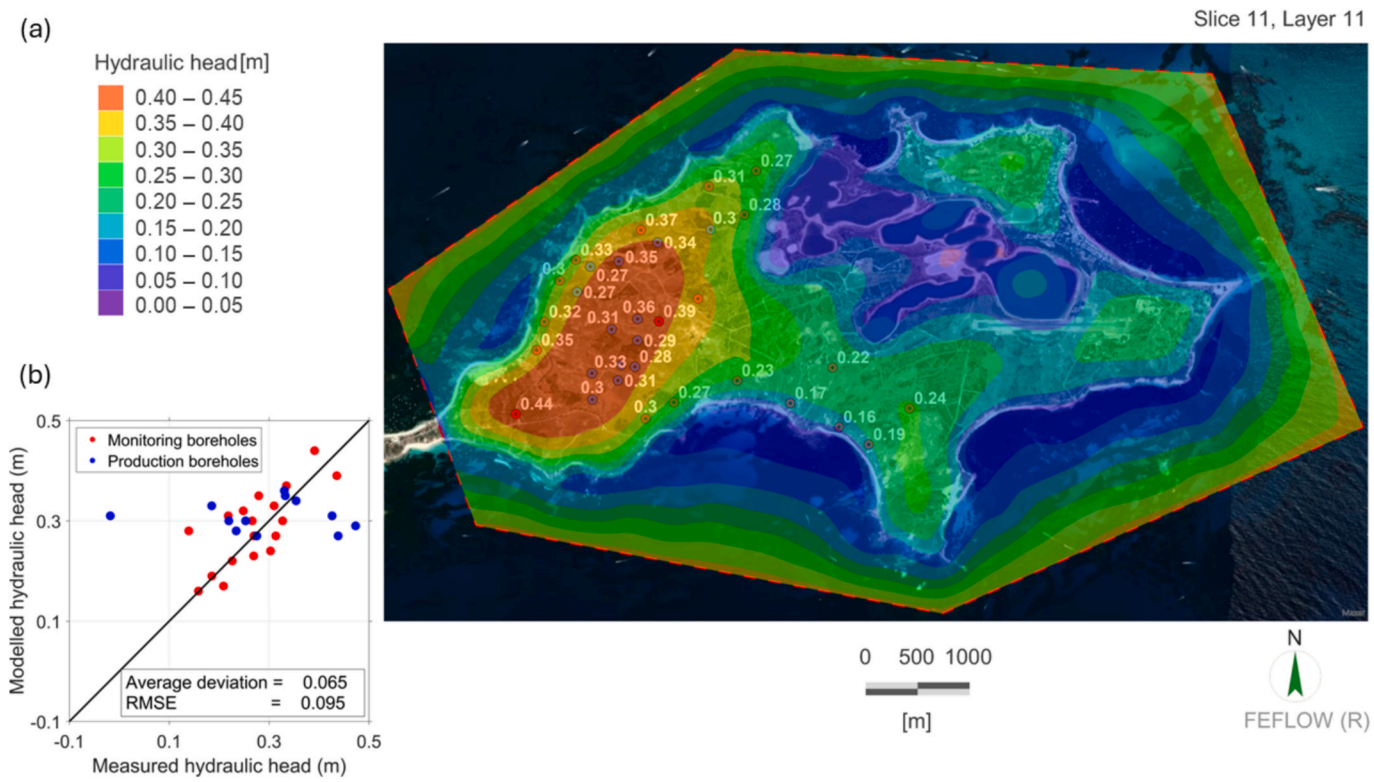

Fig. 3. (a) Colormap representing equivalent freshwater hydraulic head distribution for slice 11 which corresponds to the zero elevation for most of the island domain and up to 5 m below the ocean floor for the buffer area. Observed heads appear in white text to enable visual comparison with model results. (b) scatter plot comparing modelled and measured hydraulic heads for monitoring (red circles) and production (blue circles) boreholes. (For interpretation of the references to colour in this figure legend, the reader is referred to the web version of this article.)

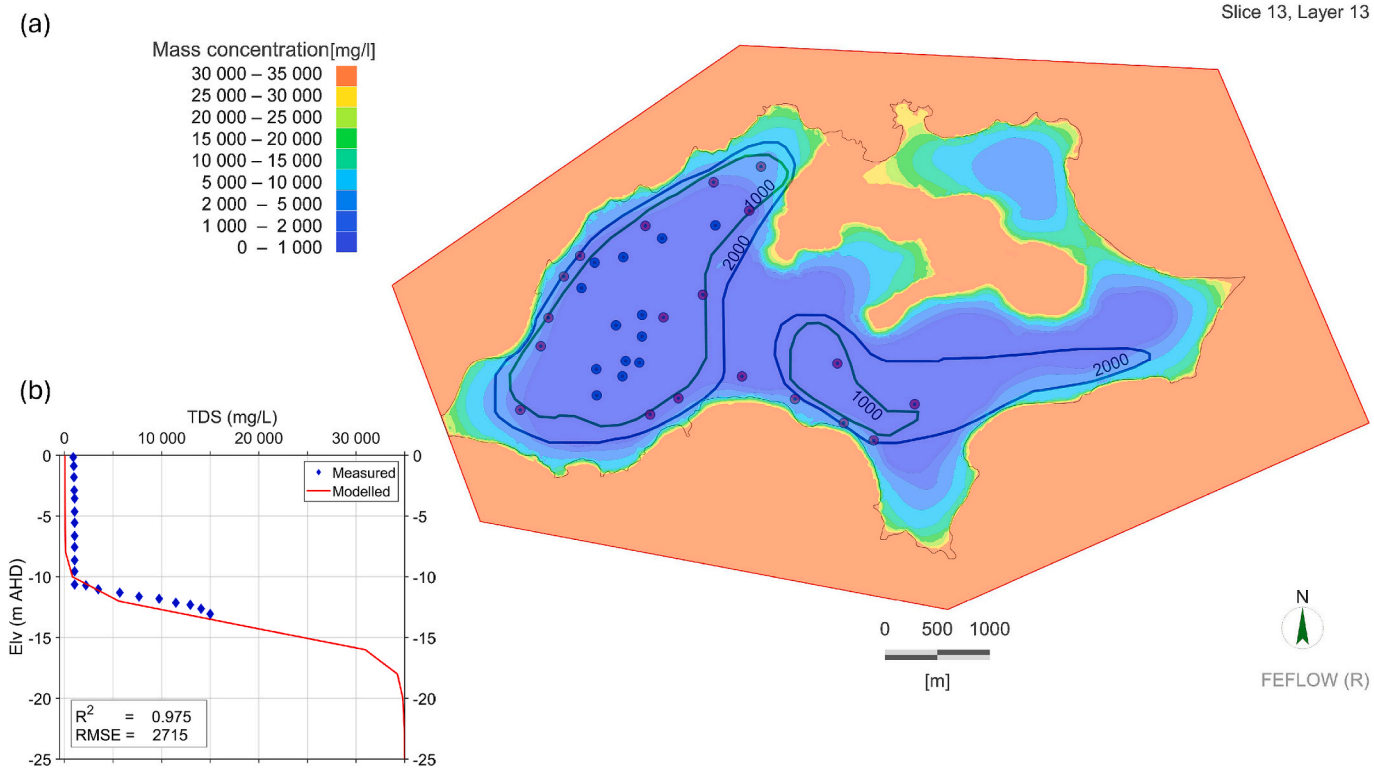

Fig. 4. (a) TDS distribution map of the upper 5 m groundwater obtained from the groundwater model in steady state and compared to 1000 and 2000 mg/L contours from 1976 (solid lines (Playford, 2004). (b) The vertical profile comparing the modelled TDS profile (red line) with the measured values (blue diamonds) for borehole W02-76 in September 1976. Values of RMSE = 2,715 mg/L and $R^2 = 0.975$ in (b) represent the goodness of fit for the TDS profile. (For interpretation of the references to colour in this figure legend, the reader is referred to the web version of this article.)

3.1.3. Phase 3: transient calibration and model validation

The equilibrium state from phase 2 was used as initial condition for transient historical matching. The daily groundwater recharge time series obtained from the water balance model was applied to the top of the island domain and groundwater abstraction was considered for pumping bores. The transient simulation covered the period from September 1976 to March 2016. We validated the calibrated parameters in this phase by transient historical matching (1976–2016) and ran two sensitivity tests varying the hydraulic anisotropy ratio to assess impacts on TDS and mean groundwater age. Fig. 5 compares the predicted values of TDS obtained from the transient model against the point measurements of TDS at three different times. Fig. 5b represents April 1992 as the period before the desalination plant operations commence. Fig. 5c corresponds to June 1995, and Fig. 5d shows March 2016, selected to represent the period covered by the recent field campaign. Relative to the calibrated anisotropy of 250 (125:0.50; RMS in Fig. 5b–d), increasing the ratio to 500 raised the pooled TDS RMS to 7,650 mg/L (1992), 5,090 mg/L (1995), and 5,250 mg/L (2016) and noticeably degraded the fit to the observed vertical TDS profiles.

The modelled TDS values closely match the measured ones for most of the boreholes, with the exception of boreholes W11-90, W27-90 and W23-90 (2016). Measurements indicate that the salinity in boreholes W11-90 and W27-90 had significantly increased by March 2016 (Fig. 5d), suggesting seawater intrusion in the island's northern section. These two boreholes are in the vicinity of production bores W01-90 and W08-90, which also experienced a change in the abstracted water from freshwater in the early 90 s (Fig. 5b) to slightly brackish in March 2016 (Fig. 5d). The increased salinity in the northern section of the lens is partially attributed to over-pumping from the production boreholes in this region (Bryan et al., 2020). Although the modelled TDS of these boreholes also shows an increase in the salinity from 1992 (Fig. 5b) to 2016 (Fig. 5d), the rate of increase is much slower than that indicated by the measurements.

The large discrepancy for borehole W23-90 which is only 400 m to the north from borehole W15-90 and nearly 10 m shallower may be explained by spatial heterogeneity in the area between the primary and secondary freshwater lenses, which was not included in our model. Point-time TDS measurements for borehole W23-90 with the mid-screen point located 5 m below msl from April 1992 (Fig. 5b) to September 1995 (Fig. 5d), ranging from 10,000 to 13,000 mg/L, are the only observations available in the western margin of this region. The exposure of Rottnest limestone to the south of the area between the primary and secondary freshwater lenses and the exposure of the Herchell limestone in its northern perimeter (Playford, 2004), i.e., around the lakes, suggest there is substantial heterogeneity in this region. Given the strong agreement between modelled and measured TDS for most of the boreholes and the dominance of the Tamal limestone, the assumption of a homogeneous aquifer remains a justified simplification for island-scale

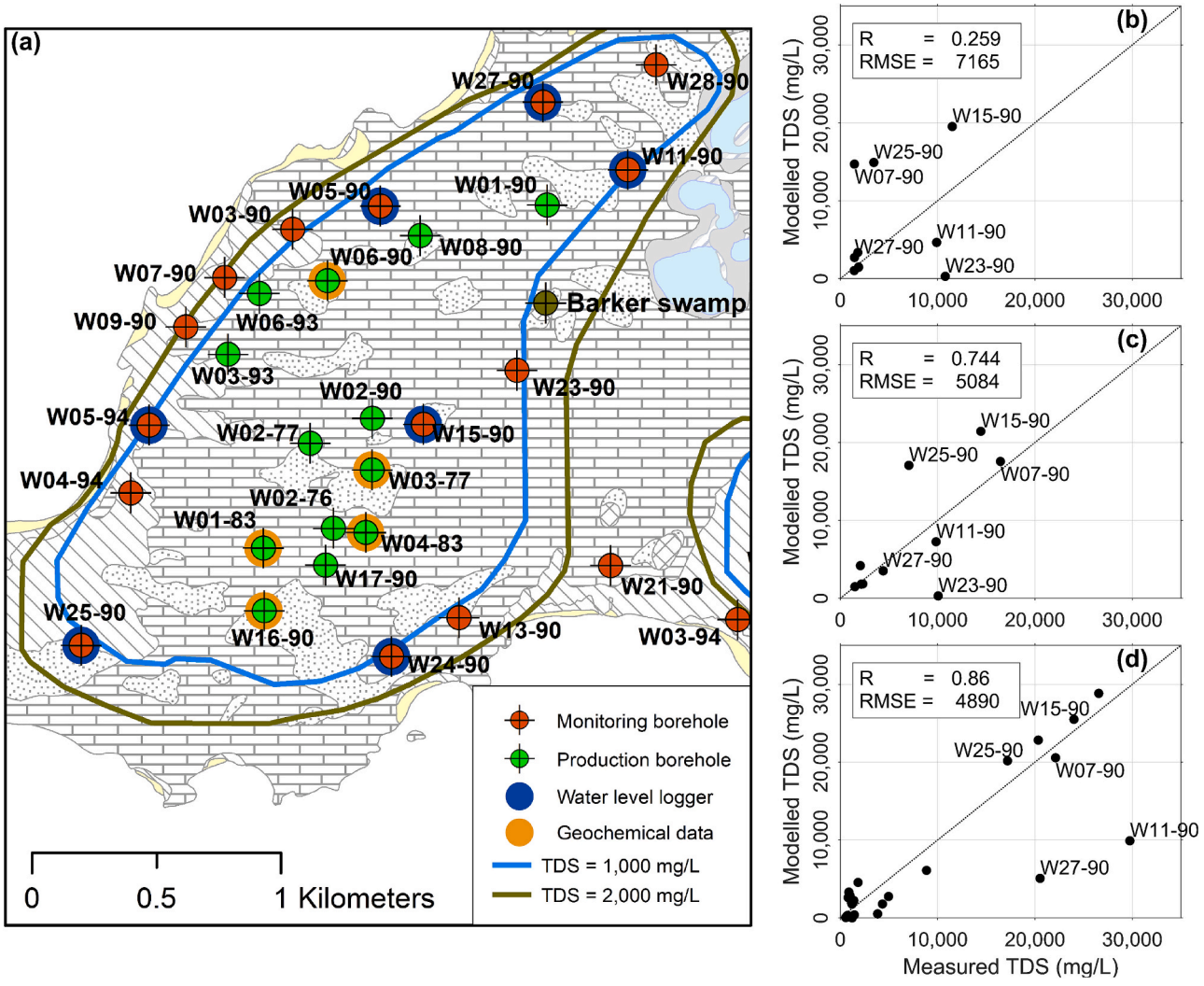

Fig. 5. Scatter plots comparing modelled TDS calculated by the transient model for April 1992 (b), June 1995 (c), and March 2016 (d) against measured values for different boreholes for which their locations are shown in (a). Both observed and modelled TDS values show a shift towards higher salinities with time.

groundwater modelling.

The measured and modelled vertical profiles of TDS for 12 boreholes were also compared at different times in Fig. S3 and Fig. S4. RMSE and Pearson correlations between the measured TDS values and modelling values at observation depths obtained using linear interpolation between simulated concentrations at regular model layers are also provided in Table S3 (see Fig. S5 for visual comparison). The comparison reveals changes in salinity in different locations across the island from September 1981 to June 1995. For most boreholes, the modelled TDS profiles closely align with their corresponding measurements both within and around the perimeter of the freshwater lens. Borehole W02-76, located in the center of the island, provides the most complete vertical TDS measurements across the salinity gradient. As shown in Fig. S3, the modelled TDS values for this borehole closely match the measured values for all periods except for minor discrepancies in October 90. Reasonable matches between modelled and measured TDS profiles were also obtained for other boreholes around the lens perimeter. However, the model results are biased at some boreholes, such as W07-90, W15-90, and W23-90 for which detailed explanations are given in the supplementary text S4.

To further constrain the calibration, groundwater ages derived using different LPMs for five production wells (Bryan et al., 2020) were compared with the corresponding modelled ages using FEFLOW. Table 1 compares the modelled mean groundwater residence time to the mean groundwater age obtained from LPMs by Bryan et al. (2020) with the age uncertainty range given in parenthesis. A sensitivity test increasing the anisotropy ration from 250 to 500 raised the mean groundwater age RMSE from 20 to 25 years.

Both LPMs and FEFLOW-derived ages indicate the presence of relatively young fresh groundwater on Rottnest Island for the selected points. However, both FEFLOW simulations and LPMs' derived estimates show a wide range of groundwater ages, indicating variability across time and space. This finding is supported by significant seasonal and spatial ^{3}H variability, which has been attributed to variations in rainfall recharge (Bryan et al., 2020). Although there are discrepancies between FEFLOW ages and LPM fresh groundwater ages, particularly at boreholes W16-90 and W03-77, where FEFLOW ages are markedly younger, the modelled ranges are broadly consistent at W01-83, W04-83, and W06-90. Overall, the differences do not show systematic bias, and the general agreement provides qualitative support for the model calibration.

Apart from the small underestimation of the rate of salination for some boreholes in northwestern part of the island, e.g., borehole W27-90 in Fig. 5, the calibration and validation results demonstrate the reliability of the developed model. Fig. 6(a) shows the TDS distribution obtained from the calibrated model for March 2016, indicating considerable lens reduction compared to the lens area delineated in 1976. The modelled TDS profile for the Northeast-Southwest (NE-SW) line also shows a reduction in the lens thickness up to 4 m compared to that obtained for 1976.

Table 1
Comparison between FEFLOW modelled groundwater residence time and the residence time derived from LPM models (Bryan et al. 2020). The LPM range indicates age variability across models and the FEFLOW range reflect the temporal variability of groundwater age during the modelling period.

Borehole	LPMs' mean residence time in years (Bryan et al., 2020) for 2014–2016	Modelled FEFLOW mean groundwater age in years for March 2016
W01-83	40.9 (15.0–61.5)	32.9 (18.1–34.5)
W16-90	39.5 (12.0–64.0)	3.3 (1.7–4.1)
W04-83	37.5 (11.5–52.4)	43.3 (16.0–62.0)
W06-90	53.3 (15.0–61.5)	43.3 (21.6–44.5)
W03-77	44.8 (17.8–64.9)	22.3 (11.5–37.7)

3.2. Transient sea level boundary conditions

Sea and groundwater level time series analyses showed that the sea level around Rottnest Island varies by more than one meter during the year. This high sea level variability can significantly affect the groundwater hydraulic head and salinity distributions. Thus, to better understand the freshwater lens response to the mixed effect of sea level and recharge variability, transient hydraulic head boundary conditions need to be considered in the modelling. To reduce the computational burden when applying a transient sea level boundary condition, we modelled a subsection of the island. While the western quadrant of the island only covers 10 % of land area, it includes more than 65 % of the lens area identified by Bryan et al. (2016) and about 40 % of the 1976 lens area. We truncated the larger model by defining groundwater divides and flow lines from the main model simulation. These were assigned as no-flow boundaries for the smaller model. The smaller model has the same mesh discretization scheme but extends only 40 m below sea level and consists of 26 vertical layers, reducing the number of elements to −10 % compared to the original model (Fig. 7).

Except for vertical hydraulic conductivity, the same aquifer properties were used, and the model was run in the same three phases as the original model (Table S3), with the two first phases providing model spin-up. Sensitivity analyses on hydraulic properties showed that using a lower vertical hydraulic conductivity (K), i.e., 0.25 m/day provides a better match between modelled and measured state variables. It is important to note that the smaller model domain represents a more geologically homogeneous subregion of the island, which, together with the scale effects (Shepley, 2024), contributed to a lower calibrated vertical hydraulic conductivity in the smaller transient model. The simulated state variables for boreholes located within the domain of the small model were then compared against their corresponding measured ones. This included the measured vertical TDS profiles of boreholes W07-90, W09-90, and W25-90 for October 1990, October 1992, and June 1995 (Fig. 8). We then compared the modelled hourly hydraulic heads for boreholes W05-94 and W25-90 against their field measurements.

Except for borehole W09-90, the modelled profiles by the small model closely resemble the observed ones for the other two boreholes. As the small version of the model does not receive the full impact of the ocean forcing along the truncated boundaries (e.g. from the other side of the island), it tends to underestimate the salinity with a larger underestimation for borehole W09-90. It should be noted that earlier measurements show higher salinity for borehole W09-90 with a minimum TDS value of 1409 mg/L in the early 90 s compared to mg/L 986 mg/L in March 2016. This trend towards fresher groundwater is inconsistent with the rest of the boreholes, suggesting a possible error in the early measurements for this specific borehole.

In the last stage of the simulation, we used hourly sea level data from the Hillarys tide gauge for the period of 10/09/2014 to 07/03/2017 as the transient hydraulic head boundary conditions for the seaside boundary of the model. To investigate the effects of variability in rainfall recharge on the hydraulic head, we ran the model under two different recharge scenarios, i.e., zero-recharge and recharge derived from a water balance model. Fig. 9 compares the modelled hydraulic head for boreholes W05-94 and W25-90 against the measured ones obtained from the real groundwater level observations.

The modelled hydraulic head for borehole 5–94 matches closely the corresponding measured ones when running the model under the zero-recharge scenario, indicating minor effects of rainfall recharge on water level fluctuations in this borehole. Bore W05-94 is only 150 m from the coast, and its groundwater level is strongly affected by sea level fluctuation as shown in Fig. 9a. Compared to borehole 5–94, modelled hydraulic heads for borehole W25-90 (Figs. 9c and d), which is located 500 m from the ocean, show a better agreement between measured and modelled groundwater levels when applying the water balance derived recharge. The modelled TDS in the vicinity of bore W05-94, however,

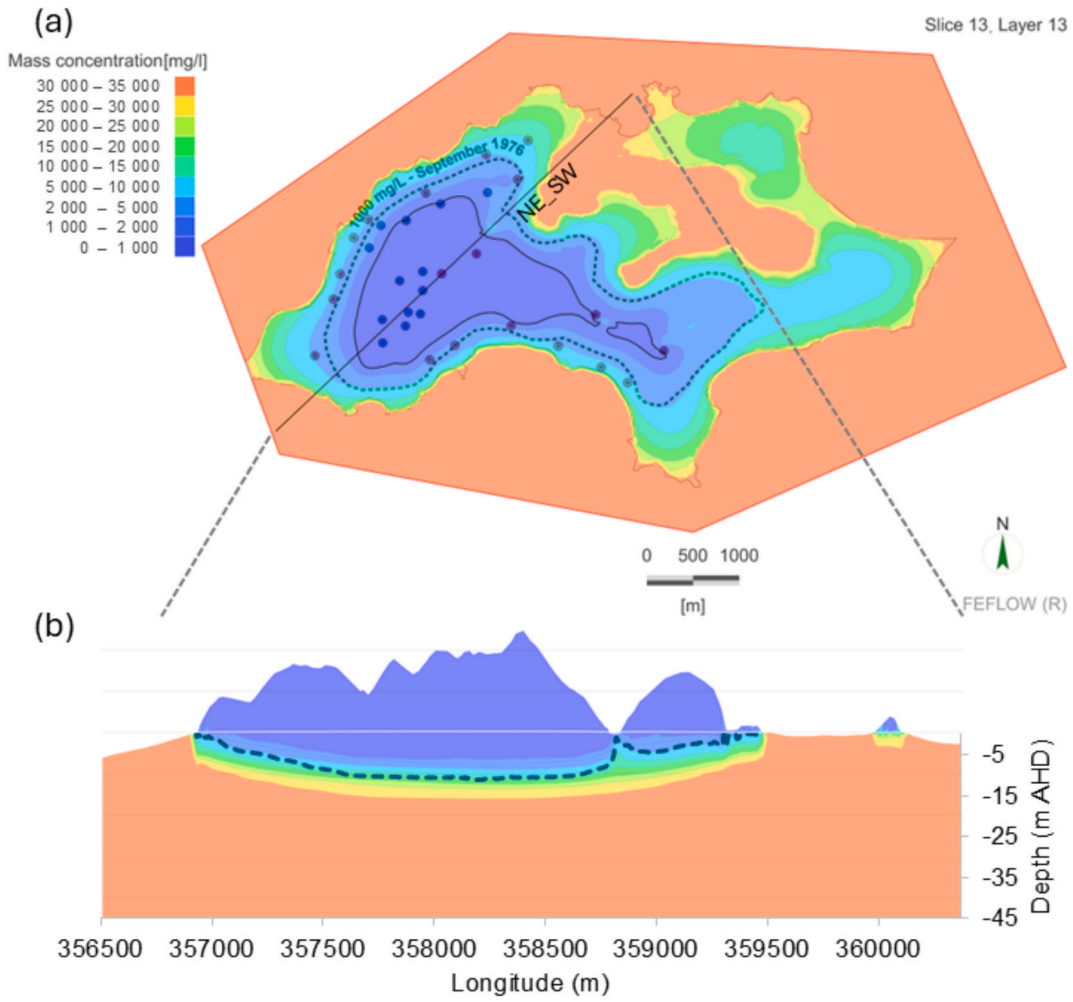

Fig. 6. (a) TDS distribution map of the upper 5 m groundwater obtained from the groundwater model in March 2016 with the dashed green labelled line showing the modelled lens area (TDS isohaline of 1,000 mg/L) for September 1976 compared to that depicted in solid black line (TDS = 1,000 mg/L) for 2016. Red circles mark monitoring boreholes while the blue ones show the location of production bores. (b) Vertical TDS distribution for the Northeast-Southwest (NE-SW) line shown in panel (a). The dashed green line shows the 1000 mg/L TDS line for September 1976. (For interpretation of the references to colour in this figure legend, the reader is referred to the web version of this article.)

significantly increases when running the model under the zero-recharge scenario. Fig. 10 shows that the thickness of the freshwater lens, i.e., depth to the 1,000 mg/L isohaline, decreases by −1.3 m by March 2017 if no recharge enters the system during the period of September 2014 to March 2017. Considering a transient hydraulic head boundary condition instead of a constant head boundary reveals the impact of sea level fluctuations on the thickness of the freshwater lens in the same location. These fluctuations not only decrease the thickness of the lens by about 0.5 m but also result in a wider transition zone as shown by the vertical position of the 10 %, 50 %, and the 90 % normalized TDS isohalines (Fig. 10e).

Fig. 10b shows the TDS difference field, with positive values (greens) indicating higher salinity for the variable sea-level boundary (SL TDS > Cnt TDS). Two green areas are located on either side of a thin blue band, i.e., negative salinity difference (SL TDS < Cnt TDS). This indicates that the fluctuating sea level stirs the interface and makes the mixing zone thicker. The enhanced dispersion and a wider mixing zone for oscillatory sea-level forcing is consistent with previous studies on sea-level fluctuation effects in coastal aquifers (Ataie-Ashtiani et al., 1999; Pool et al., 2014). The effects of the sea level fluctuations extend further inland, enhancing seawater intrusion near the bore W02-77 as shown in Fig. S6c. Removing the seasonal (nontidal) component from the sea level boundary reduces the inland salinization signal, showing that low-frequency (seasonal) sea level variability is the primary driver inland. As shown in Fig. 10 and Fig. S6, the combined effects of sea level fluctuations and rainfall recharge drive subsurface flow and mass transport dynamics on Rottnest Island, particularly on a seasonal time scale. Detailed analysis of this process, as shown in Fig. 10, reveals a vertical movement of the transition zone throughout the year. The vertical movement of the 1,000 mg/L TDS isohaline resulting solely from sea level fluctuation measures about 0.4 m in the proximity of borehole W05-94 (Fig. 10e). Fig. S8 shows the TDS variability in boreholes W07-90 and W25-90 resulting from transient simulation for the period of September 2014 to March 2017. Enhanced salinity during the late autumn or early winter, followed by its reduction in late Spring or early summer can be seen for both boreholes, with a higher intra-annual variability for borehole W07-90, which is closer to the coast.

4. Discussion

Freshwater lenses on small oceanic islands are susceptible to sea level and recharge changes, with most islands in the Indian Ocean experiencing freshwater lens reduction due to rainfall decline (Bryan et al., 2016; Chattopadhyay and Singh, 2013). The dynamic nature of the freshwater lenses combined with the complexity of their responses to multiple forces highlights the need for quantitative numeric

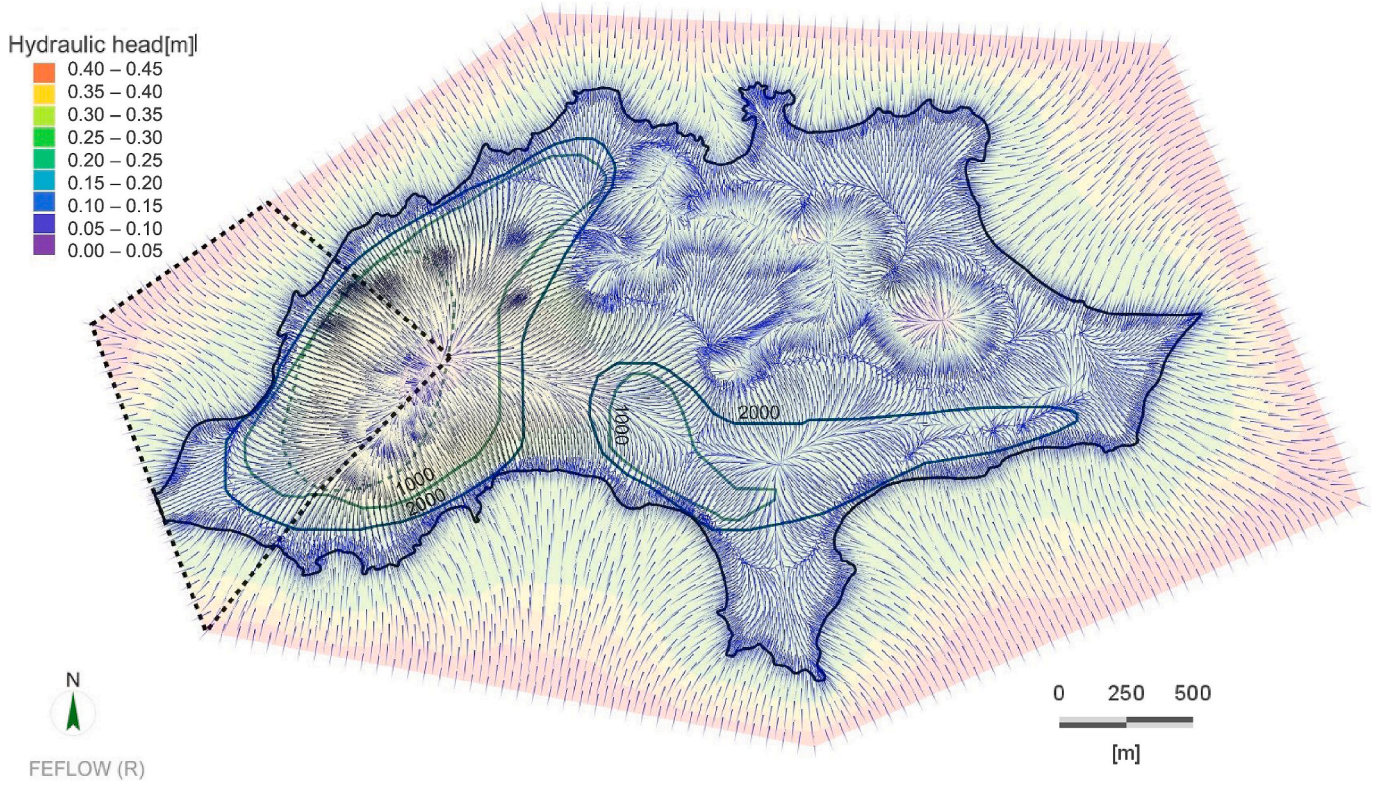

Fig. 7. Truncated area considered for the new model shown in dashed black line with the blue arrows indicating the groundwater flow lines overlain by the hydraulic head distribution map. The labelled contours show the 1976 freshwater lenses and the dashed green line indicates the lens area detected in 2016 by Bryan et al. (2016). (For interpretation of the references to colour in this figure legend, the reader is referred to the web version of this article.)

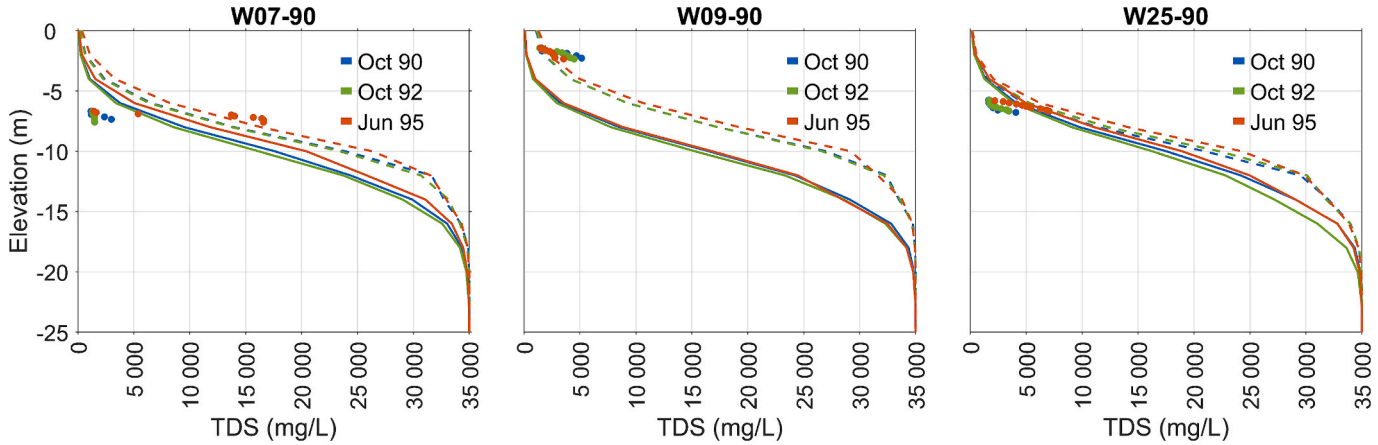

Fig. 8. Vertical profiles comparing TDS concentration produced by the small model for boreholes W07-90, W09-90, and W25-90 shown in solid lines with that by the original model (dashed lines). The coloured circles show the measurements with blue, green, and orange representing Oct 90, Oct 92, and Jun 95, respectively. (For interpretation of the references to colour in this figure legend, the reader is referred to the web version of this article.)

groundwater models to disentangle lens response to the individual forcings. However, groundwater modelling of these systems can be highly uncertain without detailed geological information and typically limited field estimations of hydraulic properties. Although a formal uncertainty analysis was not undertaken, as it would require excessive simulation time, the inclusion of multiple data sources; groundwater levels, TDS-depth profiles, and groundwater age data in the calibration of the groundwater model refined the values of the parameters utilized in the present study.

The modelled values for all three different observation types (hydraulic head, salinity and groundwater age) used for calibration in this study showed a good match with their corresponding measurements across both time and space. The TDS profiles, in particular, showed a good agreement with the available measured vertical concentrations for most monitoring boreholes (Fig. S3, Fig. S4, and Fig. 8). Consistent with the previous field study (Bryan et al., 2016), the groundwater model reveals a significant reduction in the freshwater lens extent compared to the late 1970s. The modelling results suggest up to 55 % reduction in the freshwater extent, encompassing both primary and secondary lenses, by 2016 compared to that modelled for 1976. Specifically, within the 1,000 mg/L TDS boundary line depicted by Playford (1976), the reduction rate is more than 40 %, leading to an estimated current lens area of 1.8 km^2. This reduction is more prominent in the northwestern part of the island where the seawater intrudes into the freshwater lens by

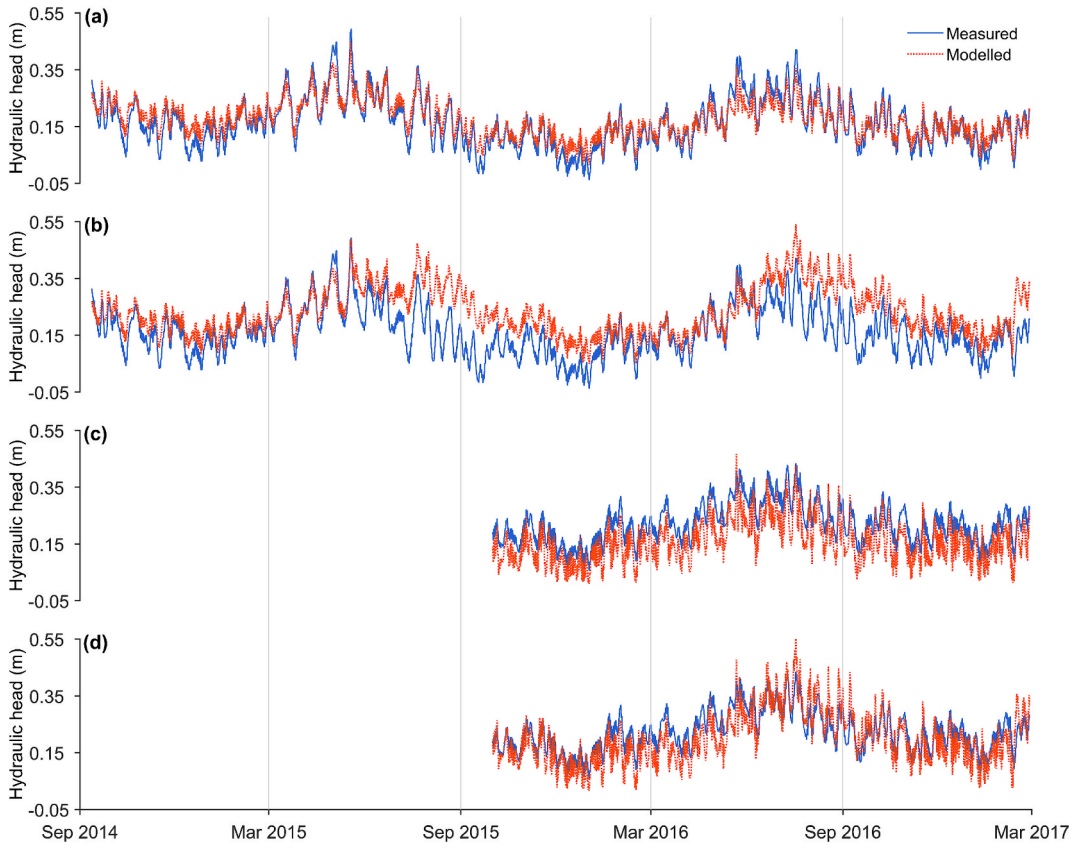

Fig. 9. (a) Zero-recharge modelled hydraulic heads against measured ones for borehole W05-94. (b) modelled hydraulic heads using the water balance derived recharge against observations for borehole W05-94. (c) and (d) same as for (a) and (b), respectively, but for borehole W25-90. A 24-hour moving average filter using a Hamming weighting function was applied on hourly time series data for a better visualization.

more than 500 m, as indicated by the position of the 1000 mg/L TDS line in March 2016 compared to its late 1976 position at the same depth (Fig. 6). Groundwater abstraction has also been suggested to play a role in seawater intrusion in this area for which detailed data on the abstraction rate is required to quantify its impact more accurately (Bryan et al., 2016).

The spatial reduction in the freshwater lens has been accompanied by a decrease in lens thickness up to −4 m (Fig. 6b) by 2016. The modelling results for 1976 and early TDS observations show a maximum thickness of −10 m for the groundwater lens at the centre of the island (Bryan et al., 2016; Playford, 1976). Due to the continued rainfall decline and potentially increased groundwater pumping activity by the early 1990s, groundwater at depths greater than 8 m gradually became slightly brackish. Although the groundwater abstraction significantly reduced after the commencing of the desalination plant in 1995, the lens thickness further decreased to no more than 6.5 m by March 2016 based on the modelling results using the rainfall recharge estimated by the water balance method. This further reduction in the lens thickness has occurred in response to the second phase of rainfall decline that started from 1999/2000 in the region (Hope et al., 2010; Priestley et al., 2023).

Rainfall recharge is the only source to replenish the groundwater lens on Rottnest Island and its long-term decline accounts for most of the lens reduction. However, a delay in the lens reduction in response to reduced recharge needs to be considered. This delay will be determined by the aquifer response time to changes in the recharge. For instance, the groundwater model shows a response time ranging from 18 to 35 years for the screen-level TDS measurements in different monitoring boreholes to reach a new steady-state condition after a 50 % reduction in the long-term mean annual recharge (Fig. S7). Combined with the estimated age of 12–18 years for the boreholes in Table 1 by Bryan et al. (2020), this study suggests a relatively short response time for the groundwater lens. However, the freshwater lens is still shrinking due to past reduction in recharge although currently at a slower rate compared to that experienced in 1990s. The lens is expected to shrink even further given the projected drier future climate for Southwest Australia (Delworth and Zeng, 2014). Although the groundwater abstraction ceased in 2017, artificial recharge activities, such as injection wells (Ríos et al., 2023), is recommended to help the freshwater lens recover.

Here we find sea level fluctuations exacerbate the impact of recharge reduction on the freshwater lens. The combined effects of sea level fluctuations and seasonal recharge lead to a vertical movement of the transition zone throughout the year, shifting upward in late May and early June when sea level is highest and with the onset of winter rainfall. This seasonal pattern highlights the critical role of winter recharge in freshening the aquifer, which increases in salinity during autumn due to the upward movement of the transition zone. Thus, although large episodic rainfall events result in significant recharge events and may influence the groundwater system on Rottnest Island (Bryan et al., 2020), they seem to have little effect on freshening the groundwater lens compared to the winter rainfall if they happen during the period of seasonal sea level rise. Tidal oscillation and wave action lead to increased dispersion and can lead to a broader transition zone, changing the groundwater salinity gradients (Guo et al., 2023; Pool et al., 2014; Rau et al., 2018). However, the tidal impact seems to be limited compared to seasonal sea level changes in the southwestern Australian region, where the mean tidal amplitude (i.e., half of the range) is only −0.2 m (Lowe et al., 2021). The lower frequency of seasonal fluctuations compared to the tidal ones allows the seasonal signal to penetrate further into the aquifer and provides enough time for mixing to occur, reinforcing the primary role of winter rainfall decline in freshwater lens reduction.

The seasonal fluctuations of inland recharge have been thought to be

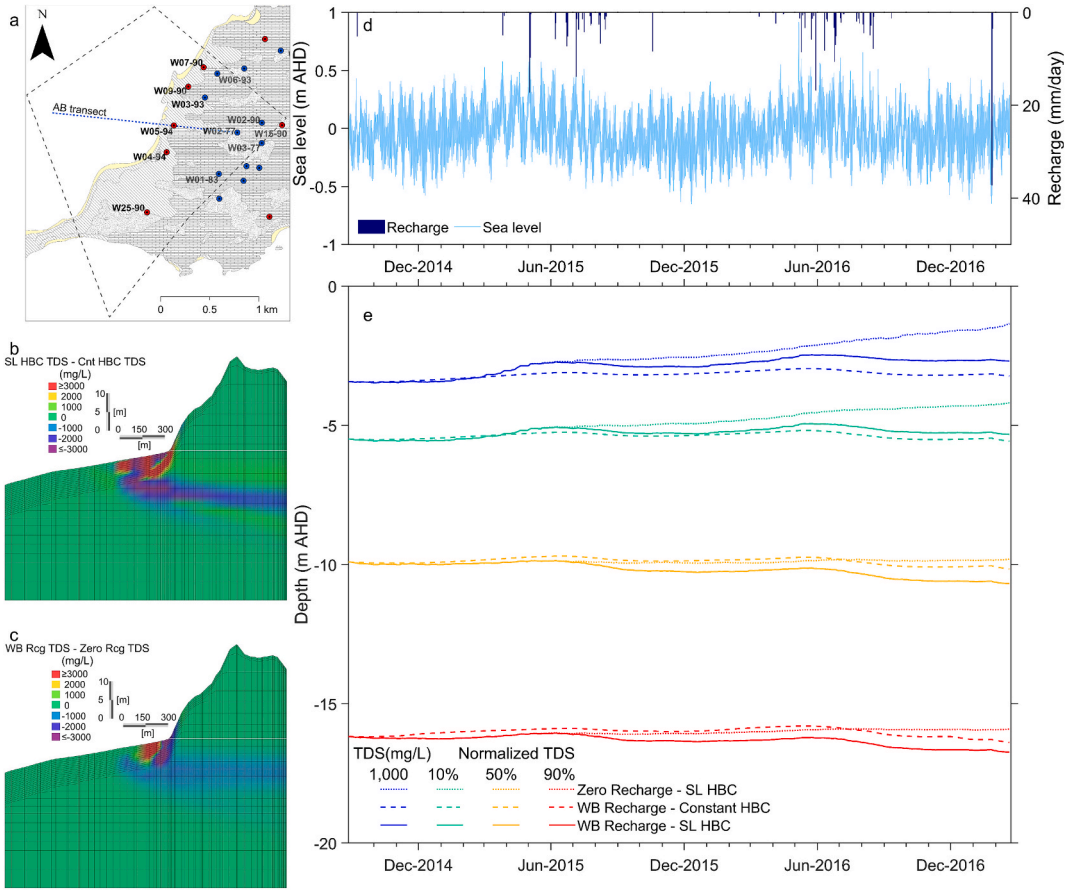

Fig. 10. (a) Locations of the monitoring and production boreholes located within the modelling domain (dashed polygon) of the smaller model. (b) Differences between the vertical TDS distributions for A-B transect shown in (a), comparing variable sea level boundary conditions (SL HBC TDS) and constant sea level conditions (Cnt HBC TDS) model runs under the Water Balance-derived (WB) recharge. (c) Same as for (b) but showing the differences between variable sea level boundary simulations under WB recharge (WB Rcg TDS) and Zero Recharge (Zero Rcg TDS) scenarios. (d) Daily groundwater recharge (vertical dark blue bars) and hourly sea level fluctuation at Hillary. (e) Vertical fluctuations of 1,000 mg/L (blue), normalized 10 % (green), normalized 50 % (orange), and normalized 90 % (red) TDS isohalines in the vicinity of the borehole W05-94. Dotted and solid lines show the simulated results under zero and WB recharge scenarios for a variable head boundary condition, while the dashed lines show the ones for a constant sea level boundary condition. Panels use AHD (Australian Height Datum) as the vertical datum. (For interpretation of the references to colour in this figure legend, the reader is referred to the web version of this article.)

the main driver for groundwater flow and salt transport in coastal aquifers (Michael et al., 2005). The modelling approach used in this study demonstrates that tidal and seasonal sea level cycles interfere with the seasonal oscillations of inland recharge, making subsurface flow and transport process more complex and dynamic. This level of complexity highlights the need to incorporate different types of groundwater data when calibrating and verifying groundwater models of freshwater lenses. The required spatial coverage of such data sets depends on the heterogeneity of the island's geology. However, it is clear from the results of this study that multi-year sub-daily groundwater level data and seasonal salinity (or salinity proxies such as TDS, chloride or specific electrical conductivity), are both required to fully understand lens dynamics in small islands.

5. Conclusion

The interaction between different forces, including oceanic, climatic, and anthropogenic forces, controls the groundwater salinity and the shape of the freshwater lens under Rottnest Island (Western Australia). The multiple forcings and the dynamic nature of the groundwater system suggests that groundwater modelling is necessary to understand and quantify the response of the freshwater lens to different stressors. However, ignoring the dynamic response of the interface by relying solely on hydraulic heads in calibrating these models provides a poorly constrained model. To overcome these limitations, different types of groundwater observations were used to constrain a 3D density-dependent groundwater model for Rottnest Island. The verification results confirmed the reliability of the developed groundwater model for predictions.

The transient model run quantified the previous findings based on field investigations regarding a significant reduction in the freshwater lens extent since its discovery in 1976. Moreover, the model revealed a shrinkage of about 4 m in the freshwater thickness since 1976, leading to approximately 50 % loss of the potable groundwater on the island by 2016 compared to 1976. Although the salinity condition at the screen depth of most of the boreholes only requires 18–38 years to stabilise, the freshwater lens has not reached a new steady-state condition due to the current drying trend in Western Australia.

The reduction in the freshwater lens on Rottnest Island is primarily due to the prolonged decline in winter rainfall across the region. Applying the transient hydraulic head boundary conditions shows that seasonal sea level fluctuations is likely to exacerbate the effects of winter rainfall decline. The amplitude and frequency of these fluctuations allow for a vertical movement of the brackish transition zone, reaching closest to the surface in late autumn and shifting downward during winter and spring recharge. Thus, winter rainfall plays a critical role in freshening the aquifer through increasing groundwater discharge to the sea when sea level decreases to its minimum height. Worryingly, the lens

reduction is still occurring, albeit at a slower rate, and it is expected to continue to occur under projected future drying, with significant impacts on the human population, biodiversity and ecosystems across the island. Globally, our study builds on an increasing body of evidence that the interplay between the climatic and oceanic forces across multiple timescales must be considered when modelling freshwater lenses in island settings to reliably quantify and predict the impacts of climate change on freshwater lenses.

CRediT authorship contribution statement

S. Sharifazari: Writing – review & editing, Writing – original draft, Visualization, Methodology, Formal analysis, Data curation, Conceptualization. **J. McCallum:** Writing – review & editing, Methodology, Data curation. **K. Meredith:** Writing – review & editing, Data curation. **F. Johnson:** Writing – review & editing, Supervision. **J.G. Palmer:** Writing – review & editing, Supervision. **C.S.M. Turney:** Writing – review & editing, Supervision. **M.S. Andersen:** Writing – review & editing, Supervision, Methodology.

Declaration of competing interest

This research was supported by the Australian Government Research Training and the UNSW Scientia PhD Scholarship Schemes. The authors declare that they have no known competing financial interests or personal relationships that could have appeared to influence the work reported in this paper.

Appendix A. Supplementary data

Supplementary data to this article can be found online at https://doi.org/10.1016/j.jhydrol.2025.134294.

Data availability

Data will be made available on request.

References

Alsumaiei, A.A., Bailey, R.T., 2018. Quantifying threats to groundwater resources in the Republic of Maldives Part I: future rainfall patterns and sea-level rise. Hydrol. Process. 32 (9), 1137–1153. https://doi.org/10.1002/hyp.11480.

Anwar, F., Wawn, P., 2013. Freshwater discharge to salt lake and its implications for freshwater management at Rottnest Island, Western Australia, Proceedings of 35th IAHR Congress 2013. International Association for Hydro-Environment Engineering and Research (IAHR), pp. 1–10.

Ataie-Ashtiani, B., Volker, R.E., Lockington, D.A., 1999. Tidal effects on sea water intrusion in unconfined aquifers. J. Hydrol. 216 (1), 17–31. https://doi.org/10.1016/S0022-1694(98)00275-3.

Banks, E.W., et al., 2024. Island hydrogeology in the tropics: Constraining a 3D variable-density groundwater flow and solute transport model with geophysics. J. Hydrol. 635, 131037. https://doi.org/10.1016/j.jhydrol.2024.131037.

Bear, J., 2004. Management of a coastal aquifer. Ground Water 42 (3), 317–318.

Briggs, M.A., et al., 2021. Small atoll fresh groundwater lenses respond to a combination of natural climatic cycles and human modified geology. Sci. Total Environ. 756, 143838. https://doi.org/10.1016/j.scitotenv.2020.143838.

Bryan, E., 2017. A multi-scale investigation of an island groundwater resource under a drying climate using isotopic techniques, UNSW Sydney.

Bryan, E., Meredith, K.T., Baker, A., Andersen, M.S., Post, V.E., 2017. Carbon dynamics in a Late Quaternary-age coastal limestone aquifer system undergoing saltwater intrusion. Sci. Total Environ. 607, 771–785.

Bryan, E., et al., 2020. How water isotopes (18O, 2H, 3H) within an island freshwater lens respond to changes in rainfall. Water Res. 170, 115301.

Bryan, E., Meredith, K.T., Baker, A., Post, V.E., Andersen, M.S., 2016. Island groundwater resources, impacts of abstraction and a drying climate: Rottnest Island, Western Australia. J. Hydrol. 542, 704–718.

Cantelon, J.A., Robinson, C.E., Kurylyk, B.L., 2023. Morphologic, atmospheric, and oceanic drivers cause multi-temporal saltwater intrusion on a remote, Sand Island. Water Resour. Res. 59 (10), e2023WR035820. https://doi.org/10.1029/2023WR035820.

Chattopadhyay, P.B., Singh, V.S., 2013. Hydrochemical evidences: vulnerability of atoll aquifers in Western Indian Ocean to climate change. Global Planet. Change 106, 123–140. https://doi.org/10.1016/j.gloplacha.2013.03.008.

Chui, T.F.M., Terry, J.P., 2013. Influence of sea-level rise on freshwater lenses of different atoll island sizes and lens resilience to storm-induced salinization. J. Hydrol. 502, 18–26. https://doi.org/10.1016/j.jhydrol.2013.08.013.

Costall, A.R., et al., 2020. Groundwater throughflow and seawater intrusion in high quality coastal aquifers. Sci. Rep. 10 (1), 9866. https://doi.org/10.1038/s41598-020-66516-6.

Delsman, J.R., Winters, P., Vandenbohede, A., Oude Essink, G.H.P., Lebbe, L., 2016. Global sampling to assess the value of diverse observations in conditioning a real-world groundwater flow and transport model. Water Resour. Res. 52 (3), 1652–1672. https://doi.org/10.1002/2014WR016476.

Delworth, T.L., Zeng, F., 2014. Regional rainfall decline in Australia attributed to anthropogenic greenhouse gases and ozone levels. Nat. Geosci. 7 (8), 583–587. https://doi.org/10.1038/ngeo2201.

Department of Water, 2014. Rottnest Island Water Reserve: Drinking Water Source Protection Plan, Government of Western Australia.

Dibaj, M., et al., 2020. Modelling seawater intrusion in the Pingtung coastal aquifer in Taiwan, under the influence of sea-level rise and changing abstraction regime. Hydrgeol. J. 28 (6), 2085–2103. https://doi.org/10.1007/s10040-020-02172-4.

Diersch, H.-J.-G., 2013. FEFLOW: finite element modeling of flow, mass and heat transport in porous and fractured media. Springer Science & Business Media.

Frederiks, R.S., Paldor, A., Carleton, G., Michael, H.A., 2024. A comparison of sea-level rise and storm-surge overwash effects on groundwater salinity of a barrier island. J. Hydrol. 644, 132050. https://doi.org/10.1016/j.jhydrol.2024.132050.

Ghassemi, F., Molson, J.W., Falkland, A., Alam, K., 1998. Three-dimensional simulation of the Home Island freshwater lens: preliminary results. Environ. Model. Software 14 (2), 181–190. https://doi.org/10.1016/S1364-8152(98)00069-3.

Goode, D.J., 1996. Direct simulation of groundwater age. Water Resour. Res. 32 (2), 289–296. https://doi.org/10.1029/95WR03401.

Guo, J., et al., 2023. Impacts of tidal oscillations on coastal groundwater system in reclaimed land. J. Mar. Sci. Eng. 11 (10), 2019.

Haehnel, P., Greskowiak, J., Robinson, C.E., Schuett, M., Massmann, G., 2023. Efficient representation of transient tidal overheight in a coastal groundwater flow model using a phase-averaged tidal boundary condition. Adv. Water Resour. 181, 104538. https://doi.org/10.1016/j.advwatres.2023.104538.

Haehnel, P., Rasmussen, T.C., Rau, G.C., 2024. Technical note: Removing dynamic sea-level influences from groundwater-level measurements. Hydrol. Earth Syst. Sci. Discuss. 2024 (28), 2767–2784. https://doi.org/10.5194/hess-28-2767-2024.

Heiss, J.W., Michael, H.A., 2014. Saltwater-freshwater mixing dynamics in a sandy beach aquifer over tidal, spring-neap, and seasonal cycles. Water Resour. Res. 50 (8), 6747–6766. https://doi.org/10.1002/2014WR015574.

Holding, S., Allen, D., 2015. From days to decades: numerical modelling of freshwater lens response to climate change stressors on small low-lying islands. Hydrol. Earth Syst. Sci. 19 (2), 933–949.

Holding, S., et al., 2016. Groundwater vulnerability on small islands. Nat. Clim. Chang. 6 (12), 1100–1103. https://doi.org/10.1038/nclimate3128.

Holt, T., Greskowiak, J., Seibert, S.L., Massmann, G., 2019. Modeling the evolution of a freshwater lens under highly dynamic conditions on a currently developing barrier island. Geofluids 2019 (1), 9484657. https://doi.org/10.1155/2019/9484657.

Holt, T., Greskowiak, J., Sültenfuß, J., Massmann, G., 2021. Groundwater age distribution in a highly dynamic coastal aquifer. Adv. Water Resour. 149. https://doi.org/10.1016/j.advwatres.2021.103850.

Hope, P., Timbal, B., Fawcett, R., 2010. Associations between rainfall variability in the southwest and southeast of Australia and their evolution through time. Int. J. Climatol. 30 (9), 1360–1371. https://doi.org/10.1002/joc.1964.

Jiao, J., Post, V., 2019. Coastal hydrogeology. Cambridge University Press.

Jurgens, B.C., Böhlke, J., Eberts, S.M., 2012. TracerLPM (Version 1): An Excel® workbook for interpreting groundwater age distributions from environmental tracer data. 2328-7055, US Geological Survey.

Leech, R.E.J., 1977. Hydrology. In: P.E. Playford and R.E.J. Leech, Geology and Hydrology of Rottnest Island. West. Australia. Geol. Survey. 6: 54-98.

Liu, J., Tokunaga, T., 2020. 3D modeling of tsunami-induced seawater intrusion and aquifer recovery in Niijima Island, Japan, under the future tsunami scenario. J. Groundw. Hydrol. 62 (2), 303–322. https://doi.org/10.5917/jagh.62.303.

Lowe, R.J., Cuttler, M.V.W., Hansen, J.E., 2021. Climatic drivers of extreme sea level events along the coastline of Western Australia. Earth's Future 9 (4), e2020EF001620. https://doi.org/10.1029/2020EF001620.

Michael, H.A., Mulligan, A.E., Harvey, C.F., 2005. Seasonal oscillations in water exchange between aquifers and the coastal ocean. Nature 436 (7054), 1145–1148. https://doi.org/10.1038/nature03935.

Pavlovskii, I., Cantelon, J.A., Kurylyk, B.L., 2022. Coastal groundwater model calibration using filtered and amplified hydraulic information retained in the freshwater–saltwater interface. Hydrgeol. J. 30 (5), 1551–1567. https://doi.org/10.1007/s10040-022-02510-8.

Playford, P., 1976. Rottnest Island: geology and groundwater potential. Western Australia Geological Survey Records, 1976.

Playford, P.E., 2004. Geology and hydrogeology of Rottnest island, Western Australia. Developments in Sedimentology 783–810. Elsevier.

Pool, M., Post, V.E.A., Simmons, C.T., 2014. Effects of tidal fluctuations on mixing and spreading in coastal aquifers: Homogeneous case. Water Resour. Res. 50 (8), 6910–6926. https://doi.org/10.1002/2014WR015534.

Priestley, S.C., et al., 2023. Caves demonstrate decrease in rainfall recharge of southwest Australian groundwater is unprecedented for the last 800 years. Commun. Earth Environ. 4 (1), 206. https://doi.org/10.1038/s43247-023-00858-7.

Puigserver, D., et al., 2024. Effects of global and climate change on the freshwater-seawater interface movement in a Mediterranean karst aquifer of Mallorca Island. Sci. Total Environ. 912, 169246. https://doi.org/10.1016/j.scitotenv.2023.169246.

Rau, G.C., Andersen, M.S., Turner, I.L., 2018. Experimental observation of increased apparent dispersion and mixing in a beach aquifer due to wave forcing. Adv. Water Resour. 119, 245–256. https://doi.org/10.1016/j.advwatres.2018.07.003.

Reznik, I.J., et al., 2021. Fresh and saline groundwater ages and flow dynamics in a perturbed coastal aquifer. J. Hydrol. 597, 125721. https://doi.org/10.1016/j.jhydrol.2020.125721.

Ríos, I.H., et al., 2023. Proposed recharge of island aquifer by deep wells with regenerated water in Gran Canaria (Spain). Groundw. Sustain. Dev. 22, 100959. https://doi.org/10.1016/j.gsd.2023.100959.

Sanford, W., 2011. Calibration of models using groundwater age. Hydrgeol. J. 19 (1), 13–16.

Schilling, O.S., Cook, P.G., Brunner, P., 2019. Beyond classical observations in hydrogeology: the advantages of including exchange flux, temperature, tracer concentration, residence time, and soil moisture observations in groundwater model calibration. Rev. Geophys. 57 (1), 146–182. https://doi.org/10.1029/2018RG000619.

Seager, R., et al., 2019. Climate variability and change of mediterranean-type climates. J. Clim. 32 (10), 2887–2915. https://doi.org/10.1175/JCLI-D-18-0472.1.

Sheng, C., et al., 2020. Evaluating dynamic mechanisms and formation process of freshwater lenses on reclaimed atoll islands in the South China Sea. J. Hydrol. 584, 124641. https://doi.org/10.1016/j.jhydrol.2020.124641.

Shepley, M.G., 2024. Vertical hydraulic conductivity and layered heterogeneity: from measurements to models. Hydrgeol. J. 32 (4), 1017–1042. https://doi.org/10.1007/s10040-024-02773-3.

Siegel, F.R., 2020. Arresting/Controlling Saltwater Contamination of Coastal Aquifers. In: Siegel, F.R. (Ed.), Adaptations of Coastal Cities to Global Warming, Sea Level Rise, Climate Change and Endemic Hazards. Springer International Publishing, Cham, pp. 5-9. doi:10.1007/978-3-030-22669-5_2.

Small, C., Nicholls, R.J., 2003. A global analysis of human settlement in coastal zones. J. Coast. Res. 584–599.

Smith, A., Massuel, S., Pollock, D., Dillon, P., 2012. Geohydrology of the Tamala Limestone Formation in the Perth region: Origin and role of secondary porosity.

Sulzbacher, H., et al., 2012. Numerical modelling of climate change impacts on freshwater lenses on the North Sea Island of Borkum using hydrological and geophysical methods. Hydrol. Earth Syst. Sci. 16 (10), 3621–3643.

Tang, Y., Singh Rathore, S., Lu, C., Luo, J., 2020. Development of groundwater lens for transient recharge in strip islands. J. Hydrol. 590, 125209. https://doi.org/10.1016/j.jhydrol.2020.125209.

Teixeira, A.M.d.A., Batista, L.V., Silva, R.M.d., Freitas, L.M.T., Santos, C.A.G., 2024. Dynamic monitoring of surface area and water volume of reservoirs using satellite imagery, computer vision and deep learning. Remote Sens. Appl.: Soc. Environ. 35, 101205. https://doi.org/10.1016/j.rsase.2024.101205.

Urdiales-Flores, D., et al., 2023. Drivers of accelerated warming in Mediterranean climate-type regions. npj Clim. Atmos. Sci. 6 (1), 97. https://doi.org/10.1038/s41612-023-00423-1.

Werner, A.D., Sharp, H.K., Galvis, S.C., Post, V.E., Sinclair, P., 2017. Hydrogeology and management of freshwater lenses on atoll islands: review of current knowledge and research needs. J. Hydrol. 551, 819–844.

White, I., Falkland, T., 2010. Management of freshwater lenses on small Pacific islands. Hydrgeol. J. 18 (1), 227–246.

Wood, C., Harrington, G.A., 2015. Influence of seasonal variations in sea level on the salinity regime of a coastal groundwater-fed wetland. Ground Water 53 (1), 90–98. https://doi.org/10.1111/gwat.12168.